Wearable Brain–Computer Interfaces Based on Steady-State Visually Evoked Potentials and Augmented Reality: A Review

Leopoldo Angrisani, *Fellow, IEEE*, Pasquale Arpaia, *Senior Member, IEEE*, Egidio De Benedetto, *Senior Member, IEEE*, Luigi Duraccio, *Graduate Student Member, IEEE*, Fabrizio Lo Regio, *Graduate Student Member, IEEE*, and Annarita Tedesco

***Abstract*—Brain–computer interfaces (BCIs) are an integration of hardware and software communication systems that allow a direct communication path between the human brain and external devices. Among the existing BCI paradigms, steady-state visually evoked potentials (SSVEPs) have gained momentum in the development of noninvasive BCI applications as they are characterized by adequate signal-to-noise ratio (SNR) and information transfer rate (ITR). In recent years, the adoption of augmented reality (AR) head-mounted displays (HMDs) to render the flickering stimuli necessary for SSVEPs elicitation has become an attractive alternative to traditional computer screens (CSs). In fact, the increase in system wearability anticipates the possibility of adopting BCIs in contexts other than research laboratory. This has contributed to a steadily-increasing interest in BCIs, as also confirmed by the recent literature dedicated to the topic. In this evolving scenario, this review intends to provide a comprehensive picture of the current state-of-the-art in relation to the latest advancement of wearable BCIs based on SSVEPs classification and AR technology. The goal is to provide the reader with a systematic comparison of different technological solutions realized over the last years, thus making future research in this direction more efficient.**

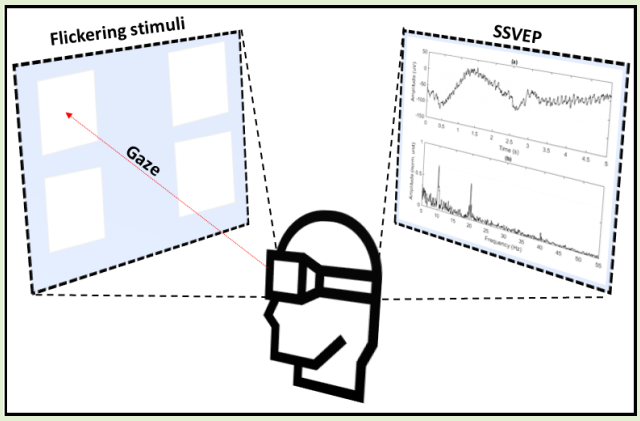

***Index Terms*— Augmented reality (AR), brain–computer interface (BCI), electroencephalography (EEG), Health 4.0, Industry 4.0, instrumentation, measurement, monitoring, steady-state visually evoked potential (SSVEP), real-time systems, wearable systems.**

I. Introduction

AS THE world embraces the 4.0 era and the digital transition [1], the demand for more sophisticated and powerful human–machine interactions is constantly increasing [2], [3]. This has fostered the diffusion of brain–computer interfaces (BCIs), a technology that integrates hardware and software solutions to enable direct communication between the human brain and external devices [4]. Basically, BCIs rely on the measurement of cerebral activity in order to associate a meaning to voluntarily or involuntarily modulated brain waves. Although BCIs are a well-known technology, it is only in recent years that their interest has been rediscovered, partly due to the advancement of technologies related to measurement systems [5]. BCIs can be classified according to different taxonomies. A first distinction can be made depending on the way brain signals are captured: functional magnetic resonance (fMRI) [6], magnetoencephalography (MEG) [7], near-infrared spectroscopy (NIRS) [8], or electroencephalography (EEG), which is commonly acknowledged as the best choice since it allows noninvasiveness, satisfactory usability, and contained costs [9]. Additionally, according to [10], BCIs can be classified as follows.

Manuscript received 12 May 2023; revised 9 June 2023; accepted 13 June 2023. Date of publication 23 June 2023; date of current version 1 August 2023. This work was supported by the Italian Ministry of University and Research (MUR) through the project "RESearch and innovation on future Telecommunications systems and networks - RESTART" (D.D: MUR no. 341, 15 March 2022), CUP: E63C22002040007. The associate editor coordinating the review of this article and approving it for publication was Dr. Wei Tang. *(Corresponding author: Egidio De Benedetto.)*

Leopoldo Angrisani, Egidio De Benedetto, and Fabrizio Lo Regio are with the Department of Electrical Engineering and Information Technology, University of Naples Federico II, 80125 Naples, Italy (e-mail: egidio.debenedetto@unina.it).

Pasquale Arpaia is with the Interdepartmental Research Center in Health Management and Innovation in Healthcare, University of Naples Federico II, 80125 Naples, Italy.

Luigi Duraccio is with the Department of Electronics and Telecommunications, Polytechnic University of Turin, 10129 Turin, Italy.

Annarita Tedesco is with the Department of Chemical Sciences, University of Naples Federico II, 80125 Naples, Italy.

Digital Object Identifier 10.1109/JSEN.2023.3287983

1) *Passive*, where the user does not directly and consciously control his electrical brainwaves. This paradigm is generally used for monitoring the user's mental state [11] and in the field of affective computing [12].
2) *Active*, where the subject voluntarily produces an appropriate modulation of the brainwaves for controlling an application, independently of external events. *Active* BCIs are arguably studied in rehabilitation protocols [13], where the most important paradigm is represented by motor imagery (MI), which is based on the premise that the neural activity within a specific region of the brain undergoes changes when subjects imagine moving any body part [14], [15], [16], [17].
3) *Reactive*, where brainwaves are produced in response to external stimuli. This peculiarity allows the use of *reactive* BCIs both for control and monitoring purposes. All event-related potentials (ERPs), including P300 [18] and visually evoked potentials (VEPs) [19], fall under this category.

Among the major *reactive* BCI paradigms [20], steady-state VEPs (SSVEPs) have rapidly gained momentum as they are characterized by adequate signal-to-noise ratio (SNR) and information transfer rate (ITR) [21]. SSVEPs are elicited in the primary visual cortex when a flickering stimulus is observed. The physiological brain response is typically inducted after a latency ranging from 80 to 160 ms [22]. It is a sinusoidal-like waveform, showing a fundamental frequency equal to that of the gazed stimulus, and often higher harmonics [23]. Stimulation frequencies typically range from 1 to 100 Hz [24]. Traditionally, these stimuli are displayed on a computer screen (CS), typically an LCD monitor placed in front of the user. This setup, which allows to visualize up to 200 stimuli [25], is very helpful for developing applications like the *BCI Speller*, a system that gives severe motor-disabled patients the possibility to communicate using their brain activity without muscular mobility [26], [27]. However, although it represents the best practice to obtain satisfactory performance, such configuration is also bulky and inevitably limits the portability of these systems. For this reason, the adoption of BCI-SSVEP has long been confined to laboratory environments [28].

Recently, innovative solutions based on the use of wireless EEG headsets and, most importantly, augmented reality (AR) head-mounted displays (HMDs) for the stimuli rendering have been considered as a promising approach to favor more wearability, immersivity, and engagement in the fruition of BCI applications [29], [30], [31], thus enabling SSVEP-based BCIs to be deployed in broader application contexts, such as healthcare [32], [33], [34] and industry [35], [36]. Nevertheless, the overall performance of such systems is strongly dependent on the specifications of the chosen HMD, which have to be thoroughly analyzed [28], [36], [37]. First, the maximum number of flickering stimuli that can be accommodated in the display depends on its field of view (FOV), and typically ranges from a minimum of two [30] up to nine [38]. However, there is much room for improvements aimed at reaching a number of stimuli comparable to LCD-based visualization. Second, the HMDs' hardware is typically less powerful than desktop PCs: this translates in a significant nonpredictability of the frame rate (frames/s) when the flickering stimuli are displayed [39]. This contribution leads to a shift in the values of the rendered stimulation frequencies. As a consequence, the classification performance of the SSVEPs could be reduced [40]. Finally, the stimuli rendered by AR HMDs are *holographic*: this means that they are superimposed on the real space, still maintaining an assigned level of transparency. Hence, if the environmental brightness increases, the SSVEPs intensity becomes weaker, leading to lower recognition [37]. For this reason, also ensuring appropriate contrast becomes a crucial aspect for AR HMDs.

Currently, the scientific community has begun to address these issues in more detail. The last five years, in fact, have seen a significant increase in works in the related literature. Fig. 1 shows the number of documents found (updated as of April 2023) after searching the keywords AR and SSVEP on the *Scopus* database. Given such a growing interest, it becomes useful to present a comprehensive review of the state-of-the-art. Therefore, this manuscript aims to review the latest developments in wearable BCIs that employ SSVEPs recognition and AR technology. This review serves a dual purpose: first, to provide readers with a detailed overview of wearable BCIs that are based on SSVEPs and AR, with a focus on the time period spanning from 2018 onward, which marks the emergence of the impact of AR advancements on the performance of SSVEP-based BCIs (as is also shown by Fig. 1). Additionally, the manuscript aims to provide a systematic comparison of the different technological solutions developed so far, by highlighting the main functional components of this particular type of BCIs.

This article is organized as follows. Section II reviews the different solutions proposed in the literature for each of the functional blocks of an AR-SSVEP BCI. Then, the related highlights are discussed in Section III. Finally, conclusions are drawn.

II. Literature Review

The typical architecture of a BCI based on SSVEPs classification and AR technology is mainly composed of four blocks, as shown in Fig. 2.

The first block concerns the *Stimuli Generation*. An AR HMD is used to run a dedicated AR application which displays N concurrent *flickering stimuli*. Each stimulus flickers at a different frequency from the others and is associated with a specific and known command to send.

The second block is related to the EEG Acquisition. A portable EEG headset acquires the user's brain signals, which are digitized by means of the EEG Processing block.

The third block is constituted by a *Processing Unit*, which can be internal to the EEG headset, or external: in the latter case, it is typically a portable board connected to the EEG headset by cable [30], or a laptop which receives the EEG samples over wireless communication [41], or even the AR HMD itself [35]. The processing unit runs the dedicated *Classification Algorithm* which is in charge to process the

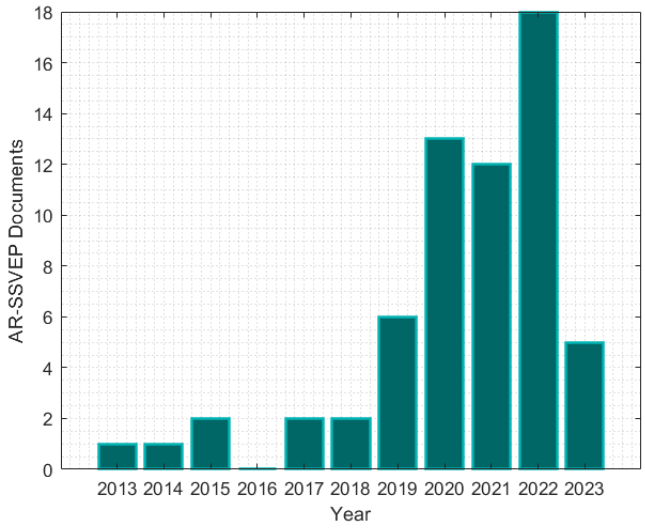

Fig. 1. Number of documents found after searching the keywords AR and SSVEP on the *Scopus* database.

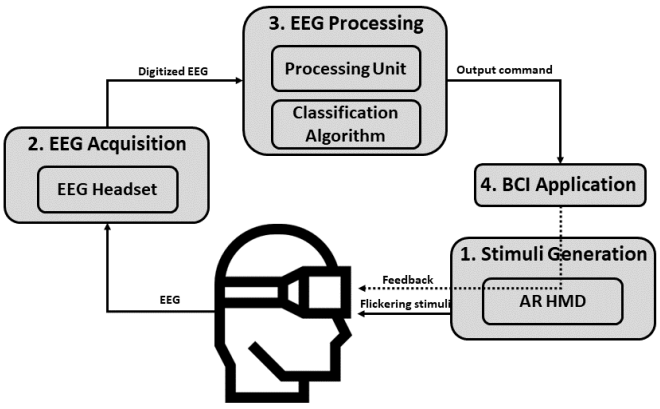

Fig. 2. Typical architecture of a BCI based on SSVEP and AR.

EEG sample and deduce which stimulus has been observed by the user: therefore, the recognition of N stimuli at different frequencies is viewed as an N-class classification problem.

Once the classification has been made, an output command is sent to the BCI application, the last block of the system which provides a *Feedback* to the user depending on the selection performed. If the classification is successful, the output command will correspond to the choice desired by the user.

In Sections II-A–II-D, for each of these functional blocks, the most recent advancement are detailed.

A. Stimuli Generation

A comprehensive characterization of the *Stimuli Generation* block can be provided on the basis of the following aspects.

1) Frequencies: According to [24], the stimulation frequencies can range from 1 to 100 Hz. Despite that, the best SNRs are typically achieved in the region from 8 to 20 Hz as discussed in [42], where 16 volunteers with normal vision were asked to participate in the experiment, and an average SSVEP amplitude response was obtained as a function of the stimulation frequency. Nevertheless, although the flickering

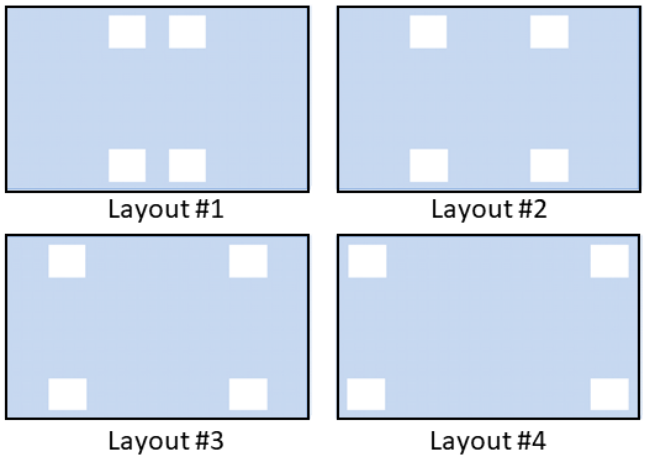

Fig. 3. Distribution of AR layouts investigated in [45].

stimuli in the given frequency range evoke SSVEPs with larger amplitude, gazing at these stimuli can result annoying and tiring for users [43]. For this reason, in recent years, the use of high-frequency stimulation was addressed by several works [43], [44], which adopted stimuli at frequencies higher than 30 Hz. However, to do this, displays with an adequate refresh rate (more than 120 Hz) are required: this places a strong limitation in AR-based SSVEP BCIs as the greatest part of AR HMDs is endowed with a 60-Hz display [41]. For this reason, different strategies to increase the user comfort were adopted by proposing innovative stimulation methods and colors (see Sections II-A3 and II-A4).

2) Layout: Since the FOV of the AR HMDs is reduced with respect to human binocular vision, the number of stimuli to accommodate in the AR display is generally low [45]. In fact, displaying in AR a number of stimuli similar to CS applications inevitably occludes the real environment, by reducing the true value of AR employment. For this reason, in [30] and [35], only two flickering stimuli were used as the FOV of the chosen AR HMD, namely Epson Moverio BT-200, was about 23°. In the last years, the improvements in AR technology allowed the development of HMDs like Microsoft HoloLens, characterized by FOV up to 52° [46]. Such HMDs are able to display from four to nine stimuli without degradation of performance [38]. Based on these considerations, an interesting aspect is represented by the choice of the stimuli layout. In [45], four different display layouts were designed to verify the influence of different layouts by comparing the resulting changes in the system performance. It resulted that the flickering stimuli should not be placed too close to each other, to avoid interference, but neither at the edges of the screen, as the angle between the user's eyes and the stimuli becomes too wide. Fig. 3 shows the four layouts investigated by the study: the configuration which allowed to achieve higher performance was the number 2. Beyond improving the visual field of AR headsets and optimizing the position of luminous stimuli, the next step toward increasing the number of visual stimuli may involve reducing their size within the display. This aspect, in the knowledge of the authors, has not yet been addressed in the context of AR-based

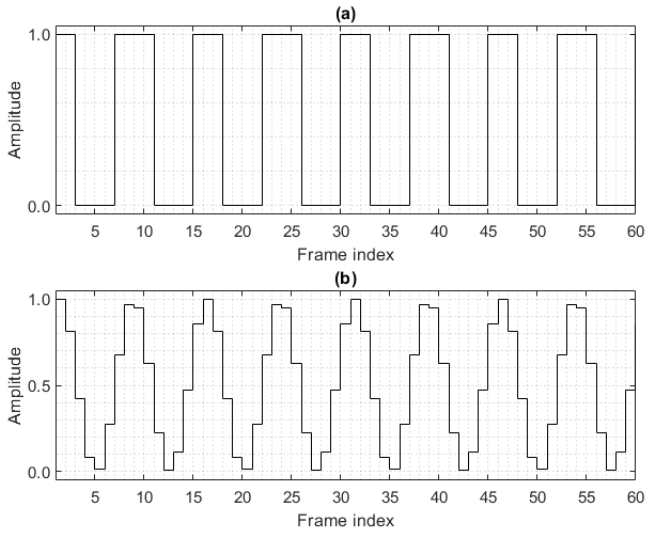

Fig. 4. Comparison between (a) *squarewave* rendering and (b) *sinewave* rendering.

Fig. 5. Likely representation of an AR environment with four flickering stimuli.

stimulation, but it is an important topic that the scientific community is beginning to explore for CS setups. For instance, in [47], the feasibility of using small and peripheral stimuli was investigated, yielding promising results.

3) Waveform: Initially, the flickering stimuli were implemented by means of simple frame alternation: each frame reversed between black and white in a cycle defined by the chosen stimulation frequency. However, in this frame-based design, the number of stimuli is always limited by the refresh rate of a the display [41], [48]. For example, on AR HMDs endowed with a 60-Hz refresh rate, the usable stimulation frequencies could only be 8.57 Hz (7 frames per cycle), 10.00 Hz (6 frames per cycle), 12.00 Hz (5 frames per cycle), or 15.00 Hz (4 frames per cycle). More generally, the stimulation frequencies can be found by the ratio RR/n, where RR is the refresh rate of the display, and n is an integer number whose values start from 2, according to the Nyquist–Shannon sampling theorem [49]. Therefore, according to this method, only subharmonic frequencies of the refresh rate could be chosen. For this reason, in [50], a new frame-based strategy was designed to render the flickering stimuli with a higher frequency resolution. This strategy also allows choosing frequencies that are not subharmonic of the refresh rate, by using a varying number of frames in each cycle. Given a desired frequency f, the stimulation sequence can be derived according to the following equation:

$$\mathrm{seq}(f, i) = \frac{1}{2} + \{1 + \mathrm{square}[2\pi f(i/\mathrm{RR})]\} \tag{1}$$

where square$(\cdot)$ generates a square wave with frequency f, i is the frame index, and RR is the refresh rate. Since the function square$(\cdot)$ allows only two values (1 or -1), it comes easy to associate the resulting highest value $[\mathrm{seq}(f, i) = 1]$ to the white color, and the lowest $[\mathrm{seq}(f, i) = 0]$ to the black one. Nevertheless, such standard ON/OFF alternation can typically be very tiring for users. For this reason, in [51], the sampled sinusoidal method was proposed, as expressed as follows:

$$\mathrm{seq}(f, i, \phi) = \frac{1}{2}\{1 + \sin[2\pi f(i/\mathrm{RR}) + \phi]\} \tag{2}$$

where $\sin(\cdot)$ generates a sine wave at the chosen frequency f and phase ϕ. Again, i and RR represent the frame index and the refresh rate, respectively. In this way, the transition from black $[\mathrm{seq}(f, i, \phi) = 0]$ to white $[\mathrm{seq}(f, i, \phi) = 1]$ is made in grayscale. In Fig. 4, a comparison between this method and the traditional ON/OFF alternation is made for a stimulation frequency of 8 Hz and a refresh rate of 60 Hz. The sampled sinusoidal method has emerged as the most widely used over the years [27].

More recently, instead, a phase-approaching (PA) method was proposed [41] to realize the flickering sequences at user-specified frequencies on AR HMDs. The sequences realized through this method (named PAS sequences) try to approximate the user-specified stimulation frequencies by means of minimizing the difference of accumulated phases between the PAS sequence and the ideal wave of user-specified frequency. Another promising approach is realizing the flickering targets by means of checkerboard-based structures, which reverse their pattern according to the chosen stimulation frequencies, as done in [52]. According to this study, the proposed layout managed to achieve an acceptable contrast relative to the environment, still maintaining adequate comfort for the user. Finally, in recent research conducted in [53] and [54], a novel type of visual stimulation known as *grow/shrink* stimulation (GSS) was introduced as a potential alternative to traditional visual stimuli. GSS involves the use of star-shaped stimuli that flicker at varying frequencies and change in size to elicit SSVEP responses. In general, the squarewave, sinewave, and PA methods employ a color alternation scheme (i.e., transitioning between black and white and vice versa) based on the selected stimulation frequency. On the other hand, the checkerboard and grow/shrink approaches rely on spatial pattern alternation, involving the inversion of color positions or changes in the icons' dimensions. These distinctions are emphasized in Table I.

TABLE I
COMPARISON BETWEEN THE DIFFERENT APPROACHES FOR IMPLEMENTING THE STIMULATIONS FOR SSVEPs INDUCTION

Method	Basic Principle	Example of Alternance
Square wave	Color Alternance	Black/White
Sinewave	Color Alternance	Modulated Black/White
Phase-Approaching	Color Alternance	Modulated Black/White
Checkerboard	Inversion of Spatial Pattern	Black/White
Grow/Shrink	Alternance of Size	Small/Large

4) Color: As the human eye is composed of three types of color-sensitive cone cells (red, green, and blue) [55], the question of which stimulation color allows to obtain the highest performance in AR-based SSVEP BCIs is meaningful. For this reason, in [56], the impact of stimulation color on the system performance was explored. Different stimulus interfaces were designed by considering four colors (white, red, green, and blue). Ten healthy subjects with normal or corrected vision were asked to participate in the experiments. Overall, the experimental results showed that the blue stimulation was considered the most comfortable interface, while red and white were seen as uncomfortable colors. However, the white color allowed to achieve the highest performance, while the blue color the lowest one. At the state-of-the-art, the white stimulus interface is most widely used in the literature [57]. Nevertheless, the trade-off between high performance and low eye fatigue has yet to be solved.

5) Frame Rate Stability: Another important aspect is the frame rate stability of the display used to render the flickering stimuli. As pointed out in [39], [58], and [59], an AR HMD typically exhibits a significant nonpredictability of the frame rate with respect to a traditional laboratory PC, as the computational unit is less powerful. This uncertainty contribution leads to an undesired shift in the frequency values of the rendered stimuli, thus increasing the possibility of misjudgment. For the sake of example, consider an AR HMD equipped with a 60-Hz display (hence, 60 frames/s), and four flickering stimuli having nominal frequency values of 11.4, 11.6, 11.8, and 12.0 Hz. If the computational effort needed to run the AR application is excessive, the frame rate of the display could decrease to 58 frames/s. Consequently, a nominal 12.0-Hz stimulus will flicker at 11.6 Hz, a nominal 11.8-Hz stimulus will flicker at 11.4 Hz, and so on. Hence, if the classification algorithm identifies 11.6 Hz as the frequency observed by the user, one might wonder whether the user really observed a frequency at 11.6 Hz, and frames/s was stable at that time, or observed a higher frequency but frames/s decreased. Currently, no hardware solutions have been proposed to solve this issue. However, in [58], a classification algorithm relying on a combined processing in frequency and time domains was proposed to estimate the frames/s variation and enhance the SSVEPs classification (see Section II-C8 for further details).

6) Environment Brightness: It should also be taken into account that the stimuli rendered by AR HMDs are *holographic* [38]. In fact, they are superimposed on the real space but, at the same time, allow the user to see what lies beyond them, as visible in Fig. 5. Therefore, the real-time SSVEPs classification can be more difficult with respect to CS-based systems. In the study conducted by Zhang and Yao [37], the effect of environment brightness on AR-SSVEP performance was investigated. Five distinct light intensities were designated as experimental conditions to replicate common ambient brightness scenarios: 0 lx (nighttime), 300 lx (learning places), 600 lx (examination rooms), 900 lx (sports venues), and 1200 lx (sunny day). In all cases, the same flickering stimuli were displayed. The obtained experimental results showed that SSVEPs can be evoked under all the tested conditions, but the response intensity became weaker when the environment brightness increased. This translates to the finding that the elicitation of SSVEP, and therefore the classification accuracy, is more effective in low ambient lighting conditions, although the higher contrast between stimuli and environment makes users feel more uncomfortable. For this reason, in the same work, an innovative SSVEP classification algorithm, named ensemble online adaptive canonical correlation analysis (eOACCA), was designed to improve the classification performance in high-brightness environment, based on iterative learning from low-light-intensity SSVEP data. Overall, the study provided a meaningful contribution to the in-depth understanding of the performance variations of AR-based SSVEP BCIs under different lighting conditions and represents a valid attempt to promote applications in challenging lighting environments by reducing eye fatigue.

7) Visual Fatigue: Finally, another crucial aspect pertains to the occurrence of visual fatigue experienced by users while observing the flickering stimuli. Similar to the conventional CS-based setup, it is an aspect that also AR-based SSVEP BCIs need to address. Several approaches have been proposed in the literature to tackle this issue. For instance, higher-frequency stimuli (above the alpha band) have been suggested as an alternative to low-frequency stimuli to mitigate the excessive visual fatigue associated with them [41], although the performance are not always satisfactory with respect to the stimulation based on the alpha band [57]. Additionally, the utilization of a dynamic time window, adapting to the subject's needs for SSVEP identification, has been demonstrated to effectively reduce the duration of visual stimulation. This reduction in time length minimizes visual fatigue by decreasing the required visual and cognitive workload [60], [61]. Furthermore, it is common in the literature to incorporate regular breaks of several minutes for users to alleviate visual fatigue [60], [61]. Moreover, similar to BCI systems based on traditional monitors, visual stimulus color plays a significant role in determining the user's visual comfort in AR-based BCIs. According to [36] and [56], it comes out that blue is the most comfortable color, while red and white are perceived as the most uncomfortable [36]. However, the performance achieved by blue are significantly worse with respect to white stimulation [56]. Finally, to objectively evaluate visual fatigue in AR SSVEP-based BCIs, questionnaires have been typically proposed thus far [29], [60]. However, it is worth noting that this approach strongly relies on subjective experience, thus lacking generalization.

B. EEG Acquisition

In the last few years, increasing attempts has been made to improve the portability of EEG acquisition systems [62]. Then,

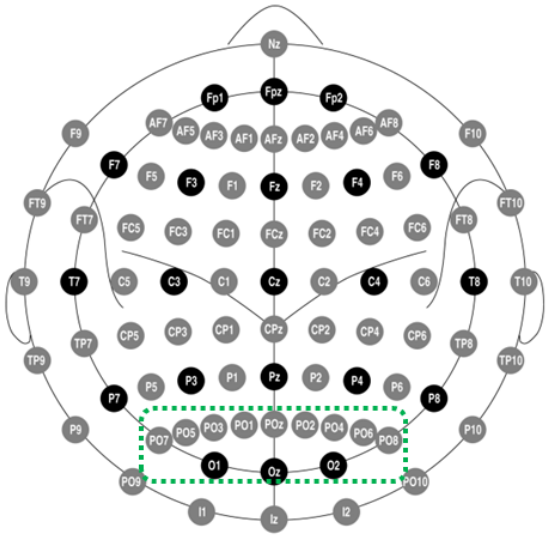

Fig. 6. User scalp according to the 10-20 International System [63]. The occipital area is bounded in green.

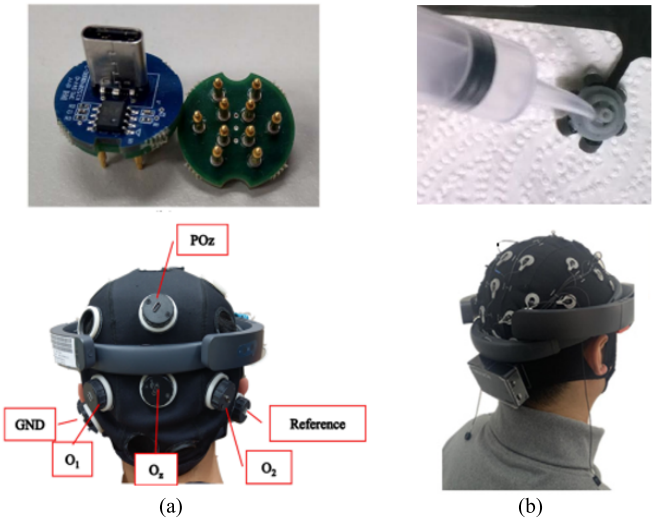

Fig. 7. Subjects wearing an AR HMD along with (a) dry EEG headset [41], and (b) wet EEG headset [56].

the most recent EEG systems are typically endowed with wireless communication to allow freedom of movement. However, the main drawbacks are the increase in communication latency and noise, and the reduced number of electrodes that can be handled. Below, an insight into the most recent developments is provided on the basis of three indicators: electrode typology, number of channels, and ergonomics.

1) Electrodes Typology: The gold standard for clinical recordings is represented by wet electrodes [64]. These are typically based on silver/silver chloride (Ag/AgCl) coating, use of conductive gels or paste, and a 1–3-mm diameter [13]. The gel ensures proper contact between skin and electrodes: this translates into low contact impedance and good SNR. However, wearing an EEG headset endowed with wet electrodes is usually a long procedure and causes annoyance for the user. Therefore, dry alternatives have been proposed [32], [41] to make the procedure faster, adopting reusable electrodes that can be easily placed to the scalp through the hair. Nevertheless, it is important to note that the contact impedance between dry electrodes and the user's scalp is highly influenced by the pressure applied to the scalp, unlike wet electrode alternatives [65]. This factor can contribute to an increase in the level of discomfort or pain experienced by users. To summarize, wet electrodes offer the best SNR, but their application requires a lengthy preparation time and can cause inconvenience for users. Another drawback is that users need to wash their hair after using wet electrodes. On the other hand, while dry electrode alternatives require a shorter preparation time and no need to wash the hair, they often induce discomfort or pain due to the applied pressure.

2) No. of Channels: Another important aspect is the number of EEG channels considered. Usually, nine or ten channels are employed [38], [39], [66], [67], typically among *PO8, PO7, PO6, PO5, PO4, PO3, POz, O2, O1, and Oz*, according to the 10-20 International System [27], [63], since SSVEPs are elicited in the primary visual cortex, which corresponds to the occipital region. However, depending on the EEG systems, also fewer channels can be considered: in [41], *Oz, O1, O2, and POz* were chosen, while in [56] they were *Oz, O1, O2, PO3, and PO4*. Instead, in [32] and [58], only the channel *Oz* was considered in an attempt to develop low-cost BCIs at the expense of reduced information gathered from the user's brain. Fig. 6 shows the user's scalp according to the 10-20 International System, by highlighting in green the occipital region.

3) Ergonomics: Finally, also the integration of EEG systems with AR HMDs represents a major challenge to improve the ergonomics of BCIs. Currently, many wet EEG headsets available on the market guarantee suitable integration with the most used AR HMDs [29], [36], [61] However, this does not apply to all the dry electrode EEG devices, which typically still have larger space requirements or limitations in terms of mobility. In Fig. 7, a successful integration of both dry and wet EEG headsets with an AR HMD is shown. As visible, dry electrodes [see Fig. 7(a)] may require more space than wet ones [see Fig. 7(b)] since amplification and filtering stages often need to be integrated to ensure proper signal acquisition [30], [41].

C. EEG Processing

An overview of the typical processing strategies for classifying SSVEPs is given as follows. Most of these strategies are employed interchangeably in both CS-based and AR-based SSVEP BCIs and are often used as baselines. However, in some cases (see Sections II-C5 and II-C8), innovative algorithms have been developed to overcome issues related to the use of AR headsets, such as frame-rate stability and contrast between the visual stimuli and the surrounding environment lighting.

1) Power Spectral Density Analysis : Power spectral density analysis (PSDA) is the most intuitive approach employed to detect and classify SSVEPs [42]. The first step is the application of a fast Fourier transform (FFT) to the user's EEG. Then, a PSD is assessed in the neighborhood of each of the *N*

rendered frequencies. Eventually, also N_h multiple harmonics can be considered, according to

$$P(f_n) = \frac{1}{2N_h k + 1}\left[\sum_{i=1}^{N_h}\sum_{j=ik_n-k}^{ik_n+k} w(i)\ A^2(j)\right] \tag{3}$$

where $P(f_n)$ is the PSD coefficient for the given frequency f_n $(n = 1, 2, \ldots, N)$, k_n is the corresponding bin in frequency domain, k is the number of nearest bins to be considered, i is the harmonics index, A is the signal amplitude, and w is a weight assigned to each harmonics. The classification is usually performed based on the hypothesis that the observed stimulus is very likely to be the one with the highest PSD [68]. The main drawback of PSDA is the requirement of a minimum time window $T_{\min}$ for the acquired EEG in order to correctly discriminate two sinusoidal tones since an appropriate frequency resolution $\Delta f = (1/T_{\min})$ is needed [69].

2) Canonical Correlation Analysis : CCA is a time domain-based method to classify SSVEPs. It is a multivariate statistical method employed to correlate linear relationships between two sets of data [70], and it is performed between the EEG signal X and a set of sine waves Y_n having the frequencies of the N stimuli rendered on the display, and eventually their multiple harmonics. Given a frequency f_n and the number of harmonics N_h, the set of sine waves $Y_n(t)$ $(n = 1, 2, \ldots, N)$ can be obtained according to the following equation:

$$Y_n = \begin{bmatrix} \sin(2\pi\ f_n\ t) \\ \cos(2\pi\ f_n\ t) \\ \sin(2\pi\ 2f_n\ t) \\ \cos(2\pi\ 2f_n\ t) \\ \cdots \\ \sin(2\pi\ N_h f_n\ t) \\ \cos(2\pi\ N_h f_n\ t) \end{bmatrix}. \tag{4}$$

For each stimulation frequency f_n, a correlation coefficient ρ_n is obtained by means of the CCA between X and Y_n. These coefficients are used for the classification stage: for the sake of example, in [70], the output of the classification was associated with the frequency having the highest correlation coefficient. Instead, in [28], [30], and [71], the maximum value among the correlation coefficients ρ_n was compared with two thresholds: the signal was classified only if the chosen correlation coefficient exceeded the thresholds. The classification performance achieved by CCA is typically better than those obtained with PSDA [68]. However, a bandpass filtering of the EEG signal can be often necessary, due to the effect of spontaneous EEG activities not involved in SSVEP events, such as eye-blinking.

3) Filter Bank Canonical Correlation Analysis : The filter bank CCA (FBCCA) method is an enhancement of CCA. It was developed in [72] and consists of three major steps: 1) filter bank analysis of the original EEG signal X; 2) CCA between SSVEP subband components and sinusoidal reference signals; and 3) signal classification. First, subband components X_{sb_j} $(j = 1, 2, \ldots, s)$ are obtained by the filter bank analysis through multiple filters with different pass-bands. Then, the standard CCA is applied to each of the subband components separately. This allows the extraction of the correlation coefficients between the subband components and the sinusoidal reference signals corresponding to the stimulation frequencies $(n = 1, 2, \ldots, N)$. In fact, a correlation value ρ_j^n is obtained for each frequency n and each subband j according to the following equation:

$$\rho^n = \left[\rho_1^n, \rho_2^n, \ldots, \rho_j^n, \ldots, \rho_s^n\right]. \tag{5}$$

Therefore, a weighted sum of squares $\tilde{\rho}^n$ is calculated among all the correlation values corresponding to the subband components

$$\tilde{\rho}^n = \sum_{j=1}^{s} w(j) \cdot \left(\rho_j^n\right)^2 \tag{6}$$

where j is the index of the subband. This represents the feature for signal classification. Since the SNR of SSVEP harmonics decreases when the response frequency increases, the weights for the subband components w are defined as follows:

$$w(j) = j^{-a} + b \tag{7}$$

where a and b are constants that maximize the classification performance and are typically determined using a grid search method in offline analysis. After that the N features $\tilde{\rho}^n$ are obtained (one for each frequency), the signal classification is finally performed based on the criterion that the observed frequency f_z $(z \in 1, \ldots, N)$ is that corresponding to the feature $\tilde{\rho}^z$ with the maximum value.

4) Extended Canonical Correlation Analysis : A different enhancement of CCA is represented by the extended CCA (xCCA) method. According to [73], xCCA combines standard CCA and Individual Template approach. Given a set of stimulation frequencies $(n = 1, 2, \ldots, N)$, the first step is to obtain the individual template $\overline{X}_n$ by averaging multiple calibration trials χ_n. Therefore, correlation coefficients between the EEG test data $\hat{X}$, the individual template $\overline{X}_n$, and sinusoidal reference Y_n are used for extracting the feature r_n. After that the N features r_n are obtained, the classification is again performed on the basis that the observed frequency f_z $(z \in 1, \ldots, N)$ corresponds to the feature r_z with the maximum value.

5) Ensemble Online Adaptive Canonical Correlation Analysis : eoACCA is a CCA-based approach that, as mentioned in Section II-A6, addresses the challenges posed by highly luminous environments in AR-based SSVEP BCIs [37]. In such scenarios, conventional methods may struggle to maintain reliable performance due to issues like strong ambient lighting and high-intensity visual stimuli. eoACCA offers a robust solution by employing an ensemble learning framework that adapts online to varying luminosity conditions. It combines multiple instances of ACCA: by aggregating the outputs of individual ACCA models, eoACCA harnesses their collective strength, enhancing overall system performance. Hence, a key feature of eoACCA is the ability to mitigate the negative effects of excessive brightness on signal quality. This is achieved through real-time updating of the ensemble weights and the fusion of correlated brain signals. Therefore, by continuously adapting to the luminosity variations, eoACCA ensures reliable

and accurate SSVEP detection, even in challenging lighting conditions.

6) Task-Related Component Analysis : Task-related component analysis (TRCA) is a widely used method proposed in [74]. Two source signals are assumed: 1) task-related signal $s(t)$ and 2) task-unrelated signal $n(t)$. Then, a linear generative model of the EEG signal $x(t)$ is considered as expressed by

$$x(t) = a_1 s(t) + a_2 n(t) \tag{8}$$

where a_1 and a_2 are coefficients that allow to project the source signals to the EEG signal. The aim is to recover the task-related signal $s(t)$ from a linear sum of observed signals $x(t)$. In this way, spatial filters W_s can be designed for removing background EEG activities from scalp recordings. Hence, a possible rule to classify SSVEPs is based on correlations of spatial-filtering-derived EEG signals [75]. More specifically, for each stimulation frequency ($n = 1, 2, \ldots, N$), the correlation coefficient c_n between the filtered EEG test data $W_s^T \hat{X}$, and the filtered individual template $W_s^T \overline{X}_n$ is extracted. Also in this case, the classification is performed by choosing the frequency associated with the highest correlation coefficient. Although TRCA-based algorithms represent a method with great potential, the main defect is that they are not able to suppress more general noises. Hence, in the study conducted in [76], a novel time filter was designed by introducing the temporally local weighting into the objective function of the TRCA-based method and using the singular value decomposition. The proposed algorithm managed to achieve results significantly better than those obtained with traditional algorithms.

7) Multivariate Synchronization Index : The multivariate synchronization index (MSI) is a method proposed in [77]. It is based on the synchronization between the input EEG signal X and a set of reference signals Y_n, where N is the number of stimulation frequencies and ($n = 1, 2, \ldots, N$). After evaluating the correlation matrix C among X and Y_n

$$C_n = \begin{bmatrix} C_{11} & C_{12} \\ C_{21} & C_{22} \end{bmatrix} \tag{9}$$

the following linear transformation is adopted to reduce the autocorrelation influence:

$$U_n = \begin{bmatrix} C_{11}^{-1/2} & 0 \\ 0 & C_{22}^{-1/2} \end{bmatrix} \tag{10}$$

then, the transformed correlation matrix is

$$R_n = U_n C_n U_n^T = \begin{bmatrix} I & C_{11}^{-1/2} C_{12} C_{22}^{-1/2} \\ C_{22}^{-1/2} C_{21} C_{11}^{-1/2} & I \end{bmatrix}. \tag{11}$$

Therefore, given the eigenvalues $\lambda_n^1, \lambda_n^2, \ldots, \lambda_n^p$ of the matrix R_n, the normalized eigenvalues are calculated as follows:

$$\overline{\lambda}_n^i = \frac{\lambda_n^i}{\mathrm{tr}(R_n)} \tag{12}$$

where $\mathrm{tr}(R_n)$ is the trace of the transformed correlation matrix R_n. Then, the synchronization index S_n is obtained by

$$S_n = 1 + \frac{\sum_{i=1}^{P} \overline{\lambda}_n^i \log\left(\overline{\lambda}_n^i\right)}{\log(P)} \tag{13}$$

where $P = N_c + 2N_h$, with N_c number of channels, and N_h number of harmonics. Finally, in the classification stage, the output frequency f_z is considered that corresponding to the maximum value among the synchronization indexes S.

8) Other Approaches: In [58], the adoption of classical machine learning (ML) classifiers such as support vector machine (SVM), k-nearest neighbor (k-NN), and artificial neural network (ANN) was addressed to mitigate the effects caused by undesired frames/s variations of AR HMDs. The proposed method, named *Features Reduction* (FR), is composed of two steps: first, the EEG signal X is processed both in frequency and time domains, in order to extract a reduced number of features. In particular, first, an FFT is applied to X; then, the actual SSVEPs peaks are detected around all the N rendered stimulus frequencies. More in detail, given a generic nominal frequency value f_n with ($n = 1, 2, \ldots, N$), the interval $[f_n \cdot 0.9, f_n \cdot 1.1]$ is considered to find the actual peak frequency f_p. Once the actual peaks are found, the resulting PSD coefficients P_n are more accurate. Thus, finally, in the time domain, the CCA between X and a set of sinewaves Y_n, having the frequencies of the N detected peaks, is performed. This also allows the CCA coefficients ρ_n obtained for each frequency to be more accurate. Ultimately, for a given brain signal composed of a number $fs \cdot T$ of EEG samples and N stimulation frequencies (where f_s is the sampling frequency, and T is time expressed in seconds), only $2N$ features are extracted and normalized. The second step is the classification, which is carried out with the aforementioned three ML classifiers, namely SVM, k-NN, and ANN. The experimental results obtained on four experimental campaigns showed a significant increase in classification performance over the traditional CCA-based algorithms, precisely owing to the mitigation of frames/s variations.

D. BCI Application

The integration of portable EEG headsets with AR HMDs has fostered new opportunities of employment of SSVEP-based BCIs in different application contexts, particularly as both light stimuli and the real world coexist in the same space: as such, this allows a better interaction between users and external devices with respect to traditional approaches.

For instance, in [30] and [32], wearable SSVEP-based BCIs were developed for the treatment of autism spectrum disorder (ASD) and attention deficit/hyperactivity disorder (ADHD). In these studies, patients were asked to control humanoid robots using an AR interface that displayed two flickering arrows superimposed onto the real world. Through this approach, the robot not only served as an educational tool but also as an extension of the patient's body, enabling augmented experiences that operated on both the perceptive-emotional and cognitive levels. However, creating a device that was highly wearable, attractive, and even playful while being reliable and training-free presented additional challenges, particularly for children under the age of eight.

Another interesting healthcare application is the control of wearable exoskeletons, which are auxiliary robots widely used in rehabilitation training. In [59], an SSVEP-based BCI with an AR interface was developed to improve the participation of stroke patients in rehabilitation training. This system was designed to reduce the patient's dependence on external stimulus equipment such as CSs while providing a more immersive experience. By integrating AR technology, the system allowed virtual and real content to coexist in the same space, minimizing the need for users to shift their attention between the computer monitor and the exoskeleton.

Further within the scope of rehabilitation, interesting applications were also developed in the field of electric wheelchair control, as shown in [52]. Since the integration of AR with SSVEP-based BCIs avoids the need for constant shifts of gaze between the visual stimuli and the real environment, the majority of participants in the experiment reported a positive experience regarding the use of the system and would recommend it to people with severe disabilities.

Instead, in [40], an integrated, real-time monitoring system based on AR and SSVEPs recognition was realized for hands-free acquisition and visualization of remote data in the Operating Room. The system allowed the anesthetist to monitor the patient's vital signs in real-time, which were acquired from the electromedical equipment, without the need to shift their attention away from the patient. This approach effectively reduced the number of interruptions to the operator's workflow, increasing their ability to promptly intervene in case of aggravating conditions of the patients.

The visualization of remote data by means of the integration of AR and SSVEP-BCIs was also exploited within the industrial framework. As an example, Angrisani et al. [35] proposed a wearable monitoring system for inspection in the context of *Industry 4.0*. This system combined AR glasses with a noninvasive, single-channel SSVEP-BCI, replacing the traditional input interface of AR platforms. The system was tested in an inspection scenario involving the collection of temperature and humidity data from sensors and displaying the results in real time on the glasses.

Another area of particular interest in industry is the control of robotic arms. Studies such as those reported in [36] and [60] demonstrated that high-level and shared control strategies based on SSVEP recognition are effective in reducing users' mental load and are preferred over direct control strategies. This preference is reinforced by the use of AR technology, which enables virtual and real content to coexist in the same space. By eliminating the need for users to shift their attention between the computer monitor and the robotic arm, AR technology can enhance the user experience.

Controlling drones [41] and humanoid robots [66], [67] for industrial tasks is a further expanding application framework. In these cases as well, the portability of AR HMDs, coupled with the high recognition performance of SSVEPs, has shown promising results in terms of the applicability of BCIs outside the research context.

Overall, all these applications have effectively harnessed the potential of AR in the BCI context. In fact, these technologies are increasingly facilitating human interaction with the surrounding sensory environment in the *4.0 Era* [31].

III. Discussion

Building upon the comprehensive literature review presented in Section II, this section aims to explicate the principal contributions and advancements in the field. As stated in Section I, the selected time horizon was from 2018 onward. Among the 56 papers found (as of April 2023) by searching the keywords AR and SSVEP on the *Scopus* Database, 20 papers (listed in Tables II–IV) are considered and thoroughly compared. The inclusion criteria were primarily based on the selection of articles published in scientific journals that clearly highlighted the main functional components of this type of BCIs, thus enabling an appropriate comparison among them. As visible, six of these works were published between 2018 and 2021, while ten of them in 2022. Finally, also four works published at the beginning of 2023 are taken into account. Each paper proposed the development of an AR-based SSVEP BCI whose architecture is consistent with the blocks defined in Fig. 2. Therefore, Tables II and III briefly describe the main features of the AR and EEG subsystems. Instead, in Table IV, the achieved results are reported in terms of ITR. The ITR represents a synthetic performance indicator able to provide the amount of information that can be conveyed to the chosen BCI application. It is defined as follows:

$$\mathrm{ITR} = \left[\log_2(N) + A\ \log_2(A) + (1-A)\ \log_2\left(\frac{1-A}{N-1}\right)\right]\frac{60}{T} \tag{14}$$

where N is the number of flickering stimuli, A is the classification accuracy in the interval [0, 1], and T is the time duration (expressed in seconds) of the EEG signals processed. It is expressed in bit/min. In order to highlight the generalization capability across people of the proposed systems, the ITR is always reported in terms of interindividual mean and, when reported in the considered works, standard deviation. As shown in (14), the ITR takes into account the trade-off between accuracy, number of stimuli, and the temporal duration of the acquired EEG. Consequently, it emerges as a more dependable metric compared to classification accuracy alone. In fact, the latter tends to be notably high when the number of stimuli is reduced and acquisition times are prolonged. Therefore, it is crucial to emphasize that achieving a high classification accuracy alone does not suffice for the development of a high-performing BCI. Optimal performance necessitates not only high accuracy but also minimized acquisition times and a substantial number of stimuli. To avoid significant misinterpretations, the classification accuracy obtained in the considered studies is not reported.

With regard to the AR Interface, as shown in Table III, the majority of the studies (13 out of 20) employed *Microsoft HoloLens 1* [81] as AR HMD. It is an AR optical-see-through (OST) device equipped with hand gestures recognition, a 60-Hz refresh rate, and a diagonal FOV of about 30°. HoloLens 1 has gained momentum in the last years as it outperformed other devices like *Epson Moverio BT-200* and *BT-35E* [82], [83], which are Smart Glasses endowed with

TABLE II
DETAILS OF THE WORKS CONSIDERED FOR DISCUSSION, ALONG WITH DETAILS OF THE EEG ACQUISITION SYSTEMS USED

Work	Year	EEG Headset	No. Channels	Electrodes type	BCI Application
Si-Mohammed et al. [29]	2018	g.USBamp	6	Wet	N/D
Park et al. [53]	2019	BioSemiActiveTwo	3	Wet	Home Appliance Control
Arpaia et al. [30]	2020	Olimex EEG-SMT	1	Dry	Driving Robots
Ke et al. [36]	2020	Micro-EEG 2	8	Wet	Robotic Arm Control
Chen et al. [60]	2021	NeuSenW	17	Wet	Robotic Arm Control
Hsu et al. [41]	2021	InMex EEG	4	Dry	Driving Drones
Sakkalis et al. [52]	2022	g.MOBILlab+	4	Wet	Wheelchair Navigation
Ravi et al. [78]	2022	g.USBamp	3	Wet	N/D
Chen, Wen et al. [79]	2022	OpenBCI Cyton	3	Wet	Wheelchair Navigation
Fang et al. [61]	2022	Neuroscan	8	Wet	Human-Robot Interaction
Du et al. [56]	2022	NeuSenW	5	Wet	N/D
Apicella et al. [58]	2022	Olimex EEG-SMT	1	Dry	N/D
Yang et al. [57]	2022	NeuSenW	8	Wet	Multi-Robot Control
Zhang, Rui et al. [39]	2022	SynAmps2	9	Wet	N/D
Zhang, Shangen et al. [66]	2022	Neuracle	9	Wet	Driving Robots
Zhao et al. [38]	2022	SynAmps2	9	Wet	N/D
Park et al. [54]	2023	BioSemiActiveTwo	12	Wet	Home Appliance Control
Zhang, Shangen et al. [67]	2023	Neuracle	9	Wet	Robot Grasping
Wang et al. [59]	2023	NuAmps	6	Wet	Exoskeleton Control
Zhang, Rui et al. [80]	2023	SynAmps2	64	Wet	N/D

TABLE III
DETAILS OF THE AR INTERFACE DEVELOPED IN THE CONSIDERED STUDIES FOR THE STIMULI GENERATION

Work	AR HMD	No. Stimuli	Frequency Range (Hz)	Stimulus type
Si-Mohammed et al. [29]	HoloLens 1	3	[10.0-15.0]	N/D
Park et al [53]	HoloLens 1	4	[7.5-12.0]	Grow/Shrink
Arpaia et al. [30]	Moverio BT-200	2	[10.0-12.0]	Square wave
Ke et al. [36]	HoloLens 1	8	[8.0-15.0]	Sinewave
Chen et al. [60]	NED+	12	[8.0-13.5]	N/D
Hsu et al. [41]	HoloLens 1	6	[19.0-29.0]	Phase-Approaching
Sakkalis et al. [52]	Moverio BT-35E	4	[6.00-8.57]	Checkerboard
Ravi et al. [78]	Homemade prototype	4	[8.0-15.0]	Square wave
Chen, Wen et al. [79]	HoloLens 2	5	[7.0-13.0]	Square wave
Fang et al. [61]	HoloLens 2	4	[9.0-15.0]	Sinewave
Du et al. [56]	HoloLens 1	4	[7.5-12.0]	Sinewave
Apicella et al. [58]	HoloLens 1	4	[8.57-15.00]	Square wave
Yang et al. [57]	Lingxi-AR	7	[8.5-14.0]	N/D
Zhang, Rui et al. [39]	HoloLens 1	25	[8.0-15.2]	Sinewave
Zhang, Shangen et al. [66]	HoloLens 1	6	[8.0-11.5]	Sinewave
Zhao et al. [38]	HoloLens 1	9	[8.0-15.2]	Sinewave
Park et al. [54]	HoloLens 1	5	[6.67-12.00]	Grow/Shrink
Zhang, Shangen et al. [67]	HoloLens 1	8	[8.0-11.5]	N/D
Wang et al. [59]	HoloLens 1	4	[7.4-11.3]	Sinewave
Zhang, Rui et al. [80]	HoloLens 1	9	[8.0-15.2]	Sinewave

a reduced diagonal FOV (23°) and that can be used only via touch-pad, thus not allowing the full exploitation of AR technology. Other AR OST devices, like *Lingxi-AR* [84] and *NED+* [85], have been used in the considered studies as an alternative to HoloLens 1, but they represent a minority within the market of AR systems. The features of HoloLens 1 allow to generate up to 25 simultaneous flickering stimuli, as conducted in [39], while the employment of Moverio BT-200 typically limits the number of stimuli only to two, like in [32], or four, like in [52]. Currently, HoloLens 1 has been discontinued and replaced by HoloLens 2 [86], [87], equipped with an improved FOV (52°), which can allow more distance between the rendered stimuli and then an increase in the achieved ITR. However, the adoption of HoloLens 2 has not been much explored so far (only in [61] and [79]), perhaps owing to a price not always affordable (currently about 3500 $) and not completely justified by the improved FOV. For the sake of comprehensiveness, an overview of the technical specifications (in terms of FOV and refresh rate) and cost of the AR HMD employed in the considered studies is provided in Table V. In almost all of the works considered in Table III, the frequencies of the flickering stimuli were chosen in the interval [8.0–15.0] Hz (commonly acknowledged as the most effective), with a stimulation type in the form of sine waves or square waves (checkerboard [52] grow/shrink templates [53], [54] currently constitute a minority). However, in [41], the frequency range employed was [19.0, 29.0 Hz], with the innovative stimulation type named PA method and previously described in Section II-A3. Instead, only in [52] and [53], frequencies below 7 Hz were considered.

Concerning the EEG Acquisition, as shown in Table II, the considerations expressed in Section II-B are confirmed: in fact, most of the considered works adopted EEG headsets endowed with wet electrodes, such as *Neuracle* [66], [67], *NeuSenW* [56], [57], *SynAmps2* [39], and BioSemi ActiveTwo [53], [54] since they guarantee a better SNR with

TABLE IV
DETAILS OF THE EEG PROCESSING STRATEGIES EMPLOYED AND RESULTS OBTAINED FROM EACH OF THE CONSIDERED STUDIES

Work	Classification Algorithm	No. Subjects	Maximum ITR (bit/min)
Si-Mohammed et al. [29]	LDA	13	62.84
Park et al. [53]	eMSI	21	37.4 ± 7.9
Arpaia et al. [30]	CCA	20	12.25 ± 6.75
Ke et al. [36]	x-CCA	14	65.50 ± 9.86
Chen et al. [60]	mtCCA-TRCA	10	67.37 ± 14.27
Hsu et al. [41]	CCA	20	131.42 ± 29.96
Sakkalis et al. [52]	CCA + LDA	12	72.3 ± 4.9
Ravi et al. [78]	CCA + CNN	6	36.97 ± 18.12
Chen, Wen et al. [79]	CCA	20	42.81
Fang et al. [61]	FB-tCNN	6	30.92 ± 9.66
Du et al. [56]	FBCCA	10	41.59 ± 5.45
Apicella et al. [58]	Features Reduction	9	33.41 ± 25.99
Yang et al. [57]	FBCCA	4	255.35 ± 21.56
Zhang, Rui et al. [39]	TRCA	13	142.05
Zhang, Shangen et al. [66]	FBCCA	12	28.91 ± 2.00
Zhao et al. [38]	CNN	10	113.39 ± 69.41
Park et al. [54]	eMSI	20	48.32
Zhang, Shangen et al. [67]	FBCCA	12	30.32
Wang et al. [59]	MSI	12	31.28 ± 6.35
Zhang, Rui et al. [80]	eOACCA	18	67.11

TABLE V
TECHNICAL SPECIFICATIONS AND COST OF THE AR HMD EMPLOYED IN THE CONSIDERED STUDIES

AR HMD	FOV (deg)	RR (Hz)	Cost ($)
Microsoft HoloLens 1 [81]	30	60	Discontinued
Microsoft HoloLens 2 [86]	52	60	≈ 3500
Epson Moverio BT-200 [82]	23	60	Discontinued
Epson Moverio BT-35E [83]	23	30	≈ 800
NED+ [86]	45	60	≈ 1400
Lingxi-AR [84]	30	60	N/D

respect to dry alternatives. The number of channels varies from a minimum of five [56] to a maximum of 64 [80], although the best practice is to consider about nine channels. However, the use of dry EEG devices like *Olimex EEG-SMT* [30], [58] and *InMex EEG* [41] represents an interesting solution in low-channel setups [32], [41], [58], where the ease of use and the reduced costs become a goal to pursue.

Finally, Table IV shows the experimental results achieved by each work. The experimental campaigns conducted in the considered studies involved on average about ten healthy volunteers with normal or corrected-to-normal vision, with some exceptions: in [30], [41], [53], [54], and [79] the participants were 20 or more, while in [57], [61], and [78] they were less than six. In the other works, they varied from 9 to 18. With regard to the classification strategies, it emerges that CCA-based algorithms are currently considered the gold standard in terms of SSVEPs classification. In fact, they were employed in 11 works out of 20: FBCCA in four works, and CCA (or x-CCA) in seven. Instead, the adoption of TRCA was addressed in two works, while MSI or extended MSI (eMSI) was used in three. The remaining works [29], [58], [60], [61] have made use of less conventional approaches. In particular, in [60], a combination between CCA and TRCA was implemented, named multitemplate CCA-TRCA (mtCCA-TRCA). Instead, in [61], an ML approach, named filter-bank temporal convolutional neural network (FB-tCNN), was developed. Another ML approach was proposed in [58], where the algorithm named FR (described in Section II-C8) represents a first attempt to mitigate the unpredictable frame rate variations of AR HMDs. Depending on the number of stimulation frequencies, number of EEG channels, and time duration, the maximum ITR achieved by the considered studies ranges from about 12 bit/min (only two flickering stimuli, one EEG channel, 2-s time duration) up to 255 bit/min (seven flickering stimuli, eight EEG channels, 0.5-s time duration).

Overall, it emerges from the considered papers that the current trends in developing highly wearable SSVEP BCIs are considering the integration of: 1) AR devices endowed with HoloLens-like specifications; 2) wet EEG headsets equipped with eight or nine channels; and 3) CCA-based classification algorithms to recognize from four to six stimulation frequencies. However, the adoption of dry EEG headsets, a reduced number of channels, and ML classification strategies is representing a sound alternative especially for low-channel and low-cost setups.

IV. CONCLUSION

In this article, a review of the literature concerning the development of BCIs based on the recognition of SSVEPs and on AR technology is provided. After showing the typical features of such systems, 20 works from 2018 onward were considered and thoroughly compared. Overall, the study conducted by the authors shows that the current developments of highly wearable SSVEP BCIs typically rely on the integration between devices like Microsoft HoloLens (which are representing the AR market leader) and wet EEG headsets equipped with about nine channels. With regard to the classification algorithms, it appears that the use of CCA-based classification algorithms is still considered the gold standard, although significant advancements based on Deep Learning are gaining attention. Instead, the adoption of dry EEG headsets along with a reduced number of channels is still confined to the role of a suitable alternative for low-cost configurations. However, this possibility to choose between different AR and EEG

subsystems is facilitating the employment of SSVEP-based BCIs in a wide variety of application scenarios in the context of digital transformation. This plays a fundamental role in moving BCIs from research to daily life.

REFERENCES

[1] M. Xu, J. M. David, and S. H. Kim, "The fourth industrial revolution: Opportunities and challenges," *Int. J. Financial Res.*, vol. 9, no. 2, pp. 90–95, 2018.

[2] T. O. Zander and C. Kothe, "Towards passive brain–computer interfaces: Applying brain–computer interface technology to human–machine systems in general," *J. Neural Eng.*, vol. 8, no. 2, Apr. 2011, Art. no. 025005.

[3] A. Apicella et al., "Employment of domain adaptation techniques in SSVEP-based brain–computer interfaces," *IEEE Access*, vol. 11, pp. 36147–36157, 2023.

[4] J. R. Wolpaw, N. Birbaumer, D. J. McFarland, G. Pfurtscheller, and T. M. Vaughan, "Brain–computer interfaces for communication and control," *Clin. Neurophysiol.*, vol. 113, no. 6, pp. 767–791, 2002.

[5] A. Kawala-Sterniuk et al., "Summary of over fifty years with brain–computer interfaces—A review," *Brain Sci.*, vol. 11, no. 1, p. 43, Jan. 2021.

[6] Y. Li, F. Wang, Y. Chen, A. Cichocki, and T. Sejnowski, "The effects of audiovisual inputs on solving the cocktail party problem in the human brain: An fMRI study," *Cerebral Cortex*, vol. 28, no. 10, pp. 3623–3637, Oct. 2018.

[7] J. Mellinger et al., "An MEG-based brain–computer interface (BCI)," *NeuroImage*, vol. 36, no. 3, pp. 581–593, Jul. 2007.

[8] J. Shin, J. Kwon, J. Choi, and C.-H. Im, "Performance enhancement of a brain–computer interface using high-density multi-distance NIRS," *Sci. Rep.*, vol. 7, no. 1, pp. 1–10, Nov. 2017.

[9] J. R. Wolpaw et al., "Brain–computer interface technology: A review of the first international meeting," *IEEE Trans. Rehabil. Eng.*, vol. 8, no. 2, pp. 164–173, Sep. 2000.

[10] T. O. Zander, C. Kothe, S. Jatzev, and M. Gaertner, "Enhancing human–computer interaction with input from active and passive brain–computer interfaces," in *Brain-Computer Interfaces, Applying Our Minds to Human-Computer Interaction*. Berlin, Germany: Springer, pp. 181–199, 2010.

[11] A. Apicella, P. Arpaia, M. Frosolone, G. Improta, N. Moccaldi, and A. Pollastro, "EEG-based measurement system for monitoring student engagement in learning 4.0," *Sci. Rep.*, vol. 12, no. 1, p. 5857, Apr. 2022.

[12] J. Marín-Morales, C. Llinares, J. Guixeres, and M. Alcañiz, "Emotion recognition in immersive virtual reality: From statistics to affective computing," *Sensors*, vol. 20, no. 18, p. 5163, Sep. 2020.

[13] P. Arpaia, A. Esposito, A. Natalizio, and M. Parvis, "How to successfully classify EEG in motor imagery BCI: A metrological analysis of the state of the art," *J. Neural Eng.*, vol. 19, no. 3, Jun. 2022, Art. no. 031002.

[14] Y. Pei et al., "A tensor-based frequency features combination method for brain–computer interfaces," in *Proc. Cognit. Syst. Inf. Process., 6th Int. Conf., (ICCSIP)*. Suzhou, China, Springer, pp. 511–526, 2022.

[15] Y. Pei et al., "A tensor-based frequency features combination method for brain–computer interfaces," *IEEE Trans. Neural Syst. Rehabil. Eng.*, vol. 30, pp. 465–475, 2022.

[16] Y. Pei et al., "Data augmentation: Using channel-level recombination to improve classification performance for motor imagery EEG," *Frontiers Hum. Neurosci.*, vol. 15, Mar. 2021, Art. no. 645952.

[17] J. Jiang, C. Wang, J. Wu, W. Qin, M. Xu, and E. Yin, "Temporal combination pattern optimization based on feature selection method for motor imagery BCIs," *Frontiers Hum. Neurosci.*, vol. 14, p. 231, Jun. 2020.

[18] E. W. Sellers, D. J. Krusienski, D. J. McFarland, T. M. Vaughan, and J. R. Wolpaw, "A P300 event-related potential brain–computer interface (BCI): The effects of matrix size and inter stimulus interval on performance," *Biol. Psychol.*, vol. 73, no. 3, pp. 242–252, Oct. 2006.

[19] G. Bin, X. Gao, Z. Yan, B. Hong, and S. Gao, "An online multi-channel SSVEP-based brain–computer interface using a canonical correlation analysis method," *J. Neural Eng.*, vol. 6, no. 4, Aug. 2009, Art. no. 046002.

[20] R. Abiri, S. Borhani, E. W. Sellers, Y. Jiang, and X. Zhao, "A comprehensive review of EEG-based brain–computer interface paradigms," *J. Neural Eng.*, vol. 16, no. 1, Feb. 2019, Art. no. 011001.

[21] M. Cheng, X. Gao, S. Gao, and D. Xu, "Design and implementation of a brain–computer interface with high transfer rates," *IEEE Trans. Biomed. Eng.*, vol. 49, no. 10, pp. 1181–1186, Oct. 2002.

[22] C. Jia, X. Gao, B. Hong, and S. Gao, "Frequency and phase mixed coding in SSVEP-based brain–computer interface," *IEEE Trans. Biomed. Eng.*, vol. 58, no. 1, pp. 200–206, Jan. 2011.

[23] G. R. Müller-Putz, R. Scherer, C. Brauneis, and G. Pfurtscheller, "Steady-state visual evoked potential (SSVEP)-based communication: Impact of harmonic frequency components," *J. Neural Eng.*, vol. 2, no. 4, pp. 123–130, Dec. 2005.

[24] C. S. Herrmann, "Human EEG responses to 1–100 Hz flicker: Resonance phenomena in visual cortex and their potential correlation to cognitive phenomena," *Exp. Brain Res.*, vol. 137, nos. 3–4, pp. 346–353, Apr. 2001.

[25] J. Han, M. Xu, X. Xiao, W. Yi, T.-P. Jung, and D. Ming, "A high-speed hybrid brain–computer interface with more than 200 targets," *J. Neural Eng.*, vol. 20, no. 1, Feb. 2023, Art. no. 016025.

[26] M. T. Medina-Juliá, Á. Fernández-Rodríguez, F. Velasco-Álvarez, and R. Ron-Angevin, "P300-based brain–computer interface speller: Usability evaluation of three speller sizes by severely motor-disabled patients," *Frontiers Hum. Neurosci.*, vol. 14, Oct. 2020, Art. no. 583358.

[27] Y. Wang, X. Chen, X. Gao, and S. Gao, "A benchmark dataset for SSVEP-based brain–computer interfaces," *IEEE Trans. Neural Syst. Rehabil. Eng.*, vol. 25, no. 10, pp. 1746–1752, Oct. 2017.

[28] P. Arpaia, E. De Benedetto, L. De Paolis, G. D'Errico, N. Donato, and L. Duraccio, "Performance enhancement of wearable instrumentation for AR-based SSVEP BCI," *Measurement*, vol. 196, Jun. 2022, Art. no. 111188.

[29] H. Si-Mohammed et al., "Towards BCI-based interfaces for augmented reality: Feasibility, design and evaluation," *IEEE Trans. Vis. Comput. Graph.*, vol. 26, no. 3, pp. 1608–1621, Mar. 2020.

[30] P. Arpaia, L. Duraccio, N. Moccaldi, and S. Rossi, "Wearable brain–computer interface instrumentation for robot-based rehabilitation by augmented reality," *IEEE Trans. Instrum. Meas.*, vol. 69, no. 9, pp. 6362–6371, Sep. 2020.

[31] A. Tedesco, D. Dallet, and P. Arpaia, "Augmented reality (AR) and brain–computer interface (BCI): Two enabling technologies for empowering the fruition of sensor data in the 4.0 era," in *Proc. AISEM Annu. Conf. Sensors Microsyst.*, vol. 753, 2021, pp. 85–91.

[32] P. Arpaia, C. Bravaccio, G. Corrado, L. Duraccio, N. Moccaldi, and S. Rossi, "Robotic autism rehabilitation by wearable brain–computer interface and augmented reality," in *Proc. IEEE Int. Symp. Med. Meas. Appl. (MeMeA)*, Jun. 2020, pp. 1–6.

[33] P. Arpaia, E. De Benedetto, N. Donato, L. Duraccio, and N. Moccaldi, "A wearable SSVEP BCI for AR-based, real-time monitoring applications," in *Proc. IEEE Int. Symp. Med. Meas. Appl. (MeMeA)*, Jun. 2021, pp. 1–6.

[34] P. Arpaia, S. Criscuolo, E. De Benedetto, N. Donato, and L. Duraccio, "A wearable AR-based BCI for robot control in ADHD treatment: Preliminary evaluation of adherence to therapy," in *Proc. 15th Int. Conf. Adv. Technol., Syst. Services Telecommun. (TELSIKS)*, Oct. 2021, pp. 321–324.

[35] L. Angrisani, P. Arpaia, A. Esposito, and N. Moccaldi, "A wearable brain–computer interface instrument for augmented reality-based inspection in industry 4.0," *IEEE Trans. Instrum. Meas.*, vol. 69, no. 4, pp. 1530–1539, Apr. 2020.

[36] Y. Ke, P. Liu, X. An, X. Song, and D. Ming, "An online SSVEP-BCI system in an optical see-through augmented reality environment," *J. Neural Eng.*, vol. 17, no. 1, Feb. 2020, Art. no. 016066.

[37] R. Zhang and D. Yao, "Ambient brightness issues in AR-BCI applications: Phenomenon and solutions," *TechRxiv*, 2022.

[38] X. Zhao, Y. Du, and R. Zhang, "A CNN-based multi-target fast classification method for AR-SSVEP," *Comput. Biol. Med.*, vol. 141, Feb. 2022, Art. no. 105042.

[39] R. Zhang et al., "The effect of stimulus number on the recognition accuracy and information transfer rate of SSVEP–BCI in augmented reality," *J. Neural Eng.*, vol. 19, no. 3, Jun. 2022, Art. no. 036010.

[40] P. Arpaia, E. De Benedetto, and L. Duraccio, "Design, implementation, and metrological characterization of a wearable, integrated AR-BCI hands-free system for health 4.0 monitoring," *Measurement*, vol. 177, Jun. 2021, Art. no. 109280.

[41] H. Hsu, K. Shyu, C. Hsu, L. Lee, and P. Lee, "Phase-approaching stimulation sequence for SSVEP-based BCI: A practical use in VR/AR HMD," *IEEE Trans. Neural Syst. Rehabil. Eng.*, vol. 29, pp. 2754–2764, 2021.

[42] Y. Wang, R. Wang, X. Gao, B. Hong, and S. Gao, "A practical VEP-based brain–computer interface," *IEEE Trans. Neural Syst. Rehabil. Eng.*, vol. 14, no. 2, pp. 234–240, Jun. 2006.

[43] X. Chen, B. Zhao, Y. Wang, and X. Gao, "Combination of high-frequency SSVEP-based BCI and computer vision for controlling a robotic arm," *J. Neural Eng.*, vol. 16, no. 2, Apr. 2019, Art. no. 026012.

[44] S. Ladouce, L. Darmet, J. J. Torre Tresols, S. Velut, G. Ferraro, and F. Dehais, "Improving user experience of SSVEP BCI through low amplitude depth and high frequency stimuli design," *Sci. Rep.*, vol. 12, no. 1, p. 8865, May 2022.

[45] X. Zhao, C. Liu, Z. Xu, L. Zhang, and R. Zhang, "SSVEP stimulus layout effect on accuracy of brain–computer interfaces in augmented reality glasses," *IEEE Access*, vol. 8, pp. 5990–5998, 2020.

[46] A. Palumbo, "Microsoft HoloLens 2 in medical and healthcare context: State of the art and future prospects," *Sensors*, vol. 22, no. 20, p. 7709, Oct. 2022.

[47] M. Xu, X. Xiao, Y. Wang, H. Qi, T. Jung, and D. Ming, "A brain–computer interface based on miniature-event-related potentials induced by very small lateral visual stimuli," *IEEE Trans. Biomed. Eng.*, vol. 65, no. 5, pp. 1166–1175, May 2018.

[48] D. Zhu, J. Bieger, G. Garcia Molina, and R. M. Aarts, "A survey of stimulation methods used in SSVEP-based BCIs," *Comput. Intell. Neurosci.*, vol. 2010, pp. 1–12, Mar. 2010.

[49] I. Volosyak, H. Cecotti, and A. Graser, "Optimal visual stimuli on LCD screens for SSVEP based brain–computer interfaces," in *Proc. 4th Int. IEEE/EMBS Conf. Neural Eng.*, Apr. 2009, pp. 447–450.

[50] Y. Wang and T.-P. Jung, "Visual stimulus design for high-rate SSVEP BCI," *Electron. Lett.*, vol. 46, no. 15, pp. 1057–1058, 2010.

[51] N. V. Manyakov, N. Chumerin, A. Robben, A. Combaz, M. van Vliet, and M. M. Van Hulle, "Sampled sinusoidal stimulation profile and multichannel fuzzy logic classification for monitor-based phase-coded SSVEP brain–computer interfacing," *J. Neural Eng.*, vol. 10, no. 3, Jun. 2013, Art. no. 036011.

[52] V. Sakkalis, M. Krana, C. Farmaki, C. Bourazanis, D. Gaitatzis, and M. Pediaditis, "Augmented reality driven steady-state visual evoked potentials for wheelchair navigation," *IEEE Trans. Neural Syst. Rehabil. Eng.*, vol. 30, pp. 2960–2969, 2022.

[53] S. Park, H.-S. Cha, and C.-H. Im, "Development of an online home appliance control system using augmented reality and an SSVEP-based brain–computer interface," *IEEE Access*, vol. 7, pp. 163604–163614, 2019.

[54] S. Park, J. Ha, J. Park, K. Lee, and C. Im, "Brain-controlled, AR-based home automation system using SSVEP-based brain–computer interface and EOG-based eye tracker: A feasibility study for the elderly end user," *IEEE Trans. Neural Syst. Rehabil. Eng.*, vol. 31, pp. 544–553, 2022.

[55] R. J. M. G. Tello, S. M. T. Müller, A. Ferreira, and T. F. Bastos, "Comparison of the influence of stimuli color on steady-state visual evoked potentials," *Res. Biomed. Eng.*, vol. 31, no. 3, pp. 218–231, Sep. 2015.

[56] Y. Du and X. Zhao, "Visual stimulus color effect on SSVEP-BCI in augmented reality," *Biomed. Signal Process. Control*, vol. 78, Sep. 2022, Art. no. 103906.

[57] Z. Yang, L. Bi, W. Chi, H. Shi, and C. Guan, "Brain-controlled multi-robot at servo-control level based on nonlinear model predictive control," *Complex Syst. Model. Simul.*, vol. 2, no. 4, pp. 307–321, Dec. 2022.

[58] A. Apicella et al., "Enhancement of SSVEPs classification in BCI-based wearable instrumentation through machine learning techniques," *IEEE Sensors J.*, vol. 22, no. 9, pp. 9087–9094, May 2022.

[59] F. Wang, Y. Wen, J. Bi, H. Li, and J. Sun, "A portable SSVEP-BCI system for rehabilitation exoskeleton in augmented reality environment," *Biomed. Signal Process. Control*, vol. 83, May 2023, Art. no. 104664.

[60] L. Chen et al., "Adaptive asynchronous control system of robotic arm based on augmented reality-assisted brain–computer interface," *J. Neural Eng.*, vol. 18, no. 6, Dec. 2021, Art. no. 066005.

[61] B. Fang et al., "Brain–computer interface integrated with augmented reality for human–robot interaction," *IEEE Trans. Cognit. Develop. Syst.*, early access, Jul. 28, 2022, doi: 10.1109/TCDS.2022.3194603.

[62] M. Ienca, P. Haselager, and E. J. Emanuel, "Brain leaks and consumer neurotechnology," *Nature Biotechnol.*, vol. 36, no. 9, pp. 805–810, Oct. 2018.

[63] R. Oostenveld and P. Praamstra, "The five percent electrode system for high-resolution EEG and ERP measurements," *Clin. Neurophysiol.*, vol. 112, no. 4, pp. 713–719, Apr. 2001.

[64] H. Wang et al., "Brain-controlled wheelchair review: From wet electrode to dry electrode, from single modal to hybrid modal, from synchronous to asynchronous," *IEEE Access*, vol. 9, pp. 55920–55938, 2021.

[65] M. Lopez-Gordo, D. Sanchez-Morillo, and F. Valle, "Dry EEG electrodes," *Sensors*, vol. 14, no. 7, pp. 12847–12870, Jul. 2014.

[66] S. Zhang, X. Gao, and X. Chen, "Humanoid robot walking in maze controlled by SSVEP-BCI based on augmented reality stimulus," *Frontiers Hum. Neurosci.*, vol. 16, Jul. 2022, Art. no. 908050.

[67] S. Zhang, Y. Chen, L. Zhang, X. Gao, and X. Chen, "Study on robot grasping system of SSVEP-BCI based on augmented reality stimulus," *Tsinghua Sci. Technol.*, vol. 28, no. 2, pp. 322–329, Apr. 2022.

[68] G. Hakvoort, B. Reuderink, and M. Obbink, "Comparison of psda and cca detection methods in a SSVEP-based BCI-system," Centre Telematics Inf. Technol. Univ. Twente, Enschede, The Netherlands, Tech. Rep. TR-CTIT-11-03, 2011.

[69] X. Chen, Y. Wang, M. Nakanishi, X. Gao, T.-P. Jung, and S. Gao, "High-speed spelling with a noninvasive brain–computer interface," *Proc. Nat. Acad. Sci. USA*, vol. 112, no. 44, pp. E6058–E6067, Nov. 2015.

[70] Z. Lin, C. Zhang, W. Wu, and X. Gao, "Frequency recognition based on canonical correlation analysis for SSVEP-based BCIs," *IEEE Trans. Biomed. Eng.*, vol. 53, no. 12, pp. 2610–2614, Dec. 2006.

[71] P. Arpaia, E. De Benedetto, L. De Paolis, G. D'Errico, N. Donato, and L. Duraccio, "Highly wearable SSVEP-based BCI: Performance comparison of augmented reality solutions for the flickering stimuli rendering," *Meas., Sensors*, vol. 18, Dec. 2021, Art. no. 100305.

[72] X. Chen, Y. Wang, S. Gao, T.-P. Jung, and X. Gao, "Filter bank canonical correlation analysis for implementing a high-speed SSVEP-based brain–computer interface," *J. Neural Eng.*, vol. 12, no. 4, Aug. 2015, Art. no. 046008.

[73] M. Nakanishi, Y. Wang, Y.-T. Wang, and T.-P. Jung, "A comparison study of canonical correlation analysis based methods for detecting steady-state visual evoked potentials," *PLoS ONE*, vol. 10, no. 10, Oct. 2015, Art. no. e0140703.

[74] M. Nakanishi, Y. Wang, X. Chen, Y. Wang, X. Gao, and T. Jung, "Enhancing detection of SSVEPs for a high-speed brain speller using task-related component analysis," *IEEE Trans. Biomed. Eng.*, vol. 65, no. 1, pp. 104–112, Jan. 2018.

[75] V. P. Oikonomou, "An adaptive task-related component analysis method for SSVEP recognition," *Sensors*, vol. 22, no. 20, p. 7715, Oct. 2022.

[76] J. Jin, Z. Wang, R. Xu, C. Liu, X. Wang, and A. Cichocki, "Robust similarity measurement based on a novel time filter for SSVEPs detection," *IEEE Trans. Neural Netw. Learn. Syst.*, early access, Oct. 14, 2021, doi: 10.1109/TNNLS.2021.3118468.

[77] Y. Zhang, P. Xu, K. Cheng, and D. Yao, "Multivariate synchronization index for frequency recognition of SSVEP-based brain–computer interface," *J. Neurosci. Methods*, vol. 221, pp. 32–40, Jan. 2014.

[78] A. Ravi, J. Lu, S. Pearce, and N. Jiang, "Enhanced system robustness of asynchronous BCI in augmented reality using steady-state motion visual evoked potential," *IEEE Trans. Neural Syst. Rehabil. Eng.*, vol. 30, pp. 85–95, 2022.

[79] W. Chen, S.-K. Chen, Y.-H. Liu, Y.-J. Chen, and C.-S. Chen, "An electric wheelchair manipulating system using SSVEP-based BCI system," *Biosensors*, vol. 12, no. 10, p. 772, Sep. 2022.

[80] R. Zhang et al., "Improving AR-SSVEP recognition accuracy under high ambient brightness through iterative learning," *IEEE Trans. Neural Syst. Rehabil. Eng.*, vol. 31, pp. 1796–1806, 2023.

[81] *Microsoft Hololens 1 Technical Specifications*. Accessed: Feb. 27, 2023. [Online]. Available: https://learn.microsoft.com/it-it/hololens/hololens1-hardware

[82] *Epson Moverio BT-200 Technical Specifications*. Accessed: Feb. 27, 2023. [Online]. Available: https://www.epson.com.au/products/projectoraccessories/Moverio_BT-200_Specs.asp

[83] *Epson Moverio BT-35E Technical Specifications*. Accessed: Apr. 18, 2023. [Online]. Available: https://www.electronicsdatasheets.com/datasheet/Moverio%20BT-35E%20datasheet.pdf

[84] *Lingxi-AR website*. Accessed: Feb. 27, 2023. [Online]. Available: https://www.lx-ar.com/#/

[85] *Ned+ AR website*. Accessed: Feb. 27, 2023. [Online]. Available: http://www.nedplusar.com/index.php?catid=62

[86] *Microsoft Hololens 2 Technical Specifications*. Accessed: Feb. 27, 2023. [Online]. Available: https://www.microsoft.com/en-us/hololens/hardware

[87] P. Arpaia, E. De Benedetto, L. De Paolis, G. D'Errico, N. Donato, and L. Duraccio, "Performance and usability evaluation of an extended reality platform to monitor patient's health during surgical procedures," *Sensors*, vol. 22, no. 10, p. 3908, May 2022.

Leopoldo Angrisani (Fellow, IEEE) is a Full Professor of Electrical and Electronic Measurements with the Department of Information Technology and Electrical Engineering, University of Naples Federico II, Naples, Italy, where he is also the General Manager/Director of CeSMA—Center of Advanced Measurement and Technology Services and the Chair of the Board of the Ph.D. Program ICTH—Information and Communication Technology for Health. He is currently playing a relevant role in designing and developing the strategic pillars of the national Competence Center on Industry 4.0, MedITech, led by Federico II University and geographically located in the South of Italy. His research activity is currently focused on the Internet of Things and cyber-physical measurement systems, green soft-growing sensors, measurement sustainability, measurement uncertainty, measurements for Industry 4.0, communication systems, and networks test and measurement.

Dr. Angrisani is a Fellow of the IEEE Instrumentation and Measurement and Communications Societies, the Chair for the IEEE Instrumentation and Measurement Society Italy Chapter, the Honorary Chairperson for the first (M&N 2019) and second (M&N 2022) edition of the IEEE International Symposium on Measurements and Networking, and the General Chairperson for the second edition (MetroInd4.0&IoT 2019) of the IEEE International Workshop on Metrology for Industry 4.0 and IoT 2019. He was one of the promoters of the TC-37 "Measurements and Networking" Technical Committee of the IEEE Instrumentation and Measurement Society and the General Chairperson for the first (M&N2011), second (M&N2013), third (M&N2015), and fourth edition (M&N2017) of the IEEE International Workshop on Measurements and Networking. He is a Representative of Italy in the IEC Validation Team-VT 60050 for maintenance and management of the International Electrotechnical Vocabulary, the Vice-Chair for the Italian Association "GMEE-Electrical and Electronic Measurements Group," and a member of CNIT, National Inter-university Consortium for Telecommunications, and the Technical Committee CT 1/25 "Terminology, Quantities and Units" of CEI (Italian Electrotechnical Committee). He is a Corresponding Member of the Accademia Pontaniana in Naples, the oldest Italian academy, with almost 600 years of history, which has always brought together renowned Neapolitan scholars. In 2009, he was awarded the IET Communications Premium for the paper titled "Performance measurement of IEEE 802.11b-based networks affected by narrowband interference through cross-layer measurements" (published in IET Communications, vol. 2, No. 1, January 2008). The IEEE Instrumentation and Measurement Society Italy Chapter, which he has been chairing since 2015, was awarded in 2016 the prestigious recognition "I&M Society Best Chapter Award" by the IEEE Instrumentation and Measurement Society, in 2017 the prestigious recognition "Most Improved Membership Chapter for 2016" by the IEEE Italy Section, in 2018 the prestigious recognition "Most Innovative Chapter 2018" by the IEEE Italy Section, and in 2021 the prestigious recognition "Chapter of the Year 2021" by the IEEE Region 8 (Europe, Middle East, Africa). In 2021, he received the prestigious recognition "2021 IEEE Instrumentation and Measurement Society Technical Award" with the following citation "For contributions in the advancement of innovative methods and techniques for communication systems test and measurement."

Pasquale Arpaia (Senior Member, IEEE) received the M.S. and Ph.D. degrees in electrical engineering from the University of Naples Federico II, Naples, Italy, in 1987 and 1992, respectively.

He was a Professor with the University of Sannio, Benevento, Italy. He is currently a Full Professor of Instrumentation and Measurements with the University of Naples Federico II and a Team Leader with CERN, Geneva, Switzerland. His current research interests include digital instrumentation and measurement techniques for magnets, superconductors, power converters, and cryogenics of particle accelerators, evolutionary diagnostics, distributed measurement systems, and analog-to-digital converter modeling and testing.

Dr. Arpaia was an Organizing and Scientific Committee Member for several IEEE and International Measurement Confederation (IMEKO) conferences. He is an Associate Editor of the *Computer Standards and Interfaces* (Elsevier), the Institute of Physics (IOP) *Journal of Instrumentation*, *Instruments* Multidisciplinary Digital Publishing Institute (MDPI), and the IEEE TRANSACTIONS ON ELECTRONICS PACKAGING AND MANUFACTURING. He is an Editor with the Momentum Press of the book collection *Emerging Technologies in Measurements, Instrumentation, and Sensors*. He is a plenary speaker in several scientific conferences.

Egidio De Benedetto (Senior Member, IEEE) received the M.S. degree in materials engineering and the Ph.D. degree in information engineering from the University of Salento, Lecce, Italy, in 2006 and 2010, respectively.

He was with the Institute of Microelectronics and Microsystems, National Research Council, Naples, Italy, from 2010 to 2012. From 2012 to 2019, he was a Research Fellow with the Department of Engineering for Innovation, University of Salento. Since 2019, he has been an Associate Professor with the Department of Electrical Engineering and Information Technology, University of Naples Federico II, Naples, Italy.

Luigi Duraccio (Graduate Student Member, IEEE) received the M.S. (cum laude) degree in electronic engineering from the University of Naples Federico II, Naples, Italy, in 2018.

He developed his master's thesis at CERN, Geneva, Switzerland, in the field of radiation measurement for electronics. His current research interests include applied metrology for the digital transition in industry and healthcare, measurement sustainability, cyber-physical measurement systems, and measurement uncertainty.

Fabrizio Lo Regio (Graduate Student Member, IEEE) received the M.S. (cum laude) degree in biomedical engineering from the University of Naples Federico II, Naples, Italy, in 2022.

His current research interests include electroencephalographic data acquisition and processing, augmented reality, and innovation on future telecommunications systems and networks.

Annarita Tedesco received the M.S. degree in telecommunication engineering from the University of Naples Federico II, Naples, Italy, in 2002, and the Ph.D. degree in physical sciences and engineering from the University of Bordeaux, Bordeaux, France, in 2023.

After her M.S. degree, she has been working in the research and development divisions of international technology companies, promoting strong cooperation with the academic world. She is currently with the Department of Chemical Sciences, University of Naples Federico II. Her research interests include industrial measurement, monitoring systems, AR-based measurement systems, measurements for Industry 4.0, sensor networks, human–computer interaction, and brain–computer interface.

Open Access funding provided by 'Università degli Studi di Napoli "Federico II"' within the CRUI CARE Agreement